Mechanism of Initial Seismicity Following Impoundment of the Monticello Reservoir, South Carolina

by Linyue Chen and Pradeep Talwani

Abstract Induced seismicity has been observed near Monticello Reservoir, South Carolina, since December 1977. Deployment of a seismic network before impoundment allowed for detection and accurate location of pursuant seismicity since its inception. Corroborative fault-plane solutions, together with geological and borehole data on fracture orientations, made it possible to determine the structures associated with the initial seismicity. Earlier descriptions attributed this seismicity to the undrained elastic response to impoundment of the reservoir or to a coupled poroelastic response, where diffusion of pore pressure and subsequent weakening was the predominant cause. Quantitative evaluation of strength changes at hypocentral locations of a subset of 53 well-located earthquakes that followed the initial impoundment led to the following results: (1) The rocks in the vicinity of Monticello Reservoir are critically stressed, and strength changes less than or equal to 0.1 MPa are adequate to trigger seismicity; (2) except at locations on the periphery of the reservoir, and at shallow depths within it (≤ 1 km), impoundment of the reservoir led to strengthening at hypocentral locations due to the undrained elastic effect; (3) diffusion of pore pressure is the dominant mechanism for the observed seismicity; and (4) the inferred permeability of the fractures associated with seismicity, 5×10^{-14} m^2 (50 mD), lies within the range of seismogenic permeability associated with induced seismicity.

Introduction

Seismicity induced by human activity is confined in both space and time, and its study can lead to a better understanding of the physics of earthquakes. Studies of seismicity related to impoundment of reservoirs (e.g., Simpson and Negmatullaev, 1981; Talwani, 1996), injection of fluids in a well (e.g., Zoback and Harjes, 1997; Jost *et al.*, 1998), withdrawal of fluids (Segall, 1989) and mining activity (e.g., McGarr and Wiebols, 1977; Gibowicz and Kijko, 1994; McGarr 1994), all bear evidence to the presence of critically stressed rocks in the earth's crust, wherein small stress changes induced by human activity trigger earthquakes.

Seismicity at Monticello Reservoir, South Carolina, is one of the better studied examples of reservoir induced seismicity (RIS). Seismic monitoring started in September 1977, three months before reservoir impoundment, and detailed geological, geophysical, and borehole data were obtained subsequently (South Carolina Electric & Gas Company, 1977; Talwani *et al.*, 1978, 1980; Fletcher, 1982; Hutchenson, 1982; Secor *et al.*, 1982; Zoback and Hickman, 1982; Talwani and Acree, 1987). These data have made it possible to infer the mechanisms associated with the onset of RIS (Talwani and Acree, 1984; Simpson *et al.*, 1988; Rajendran and Talwani, 1992; Talwani, 1997). All these studies address the mechanisms of RIS in a qualitative manner. Simpson *et al.* (1988) ascribe the initial seismicity to the undrained loading effect of impoundment, whereas Talwani and Acree (1984) and Talwani (1997) suggest that diffusion of pore pressure was mainly responsible. To evaluate these effects, we report the results of quantitative evaluations of the two mechanisms. First, we briefly summarize our understanding of these two effects and then evaluate the factors that led to the initial seismicity from 25 December 1977 to 31 January 1978.

Background

Impoundment of a reservoir can trigger seismicity in two ways, an immediate, undrained response to loading, and a delayed response due to the diffusion of pore pressure. (For a detailed discussion, see Simpson *et al.* [1988], Rajendran and Talwani [1992], and Talwani [1997].) Here we briefly summarize the two effects and introduce the nomenclature used in this article.

The RIS is caused by shear failure along a pre-existing fault plane. According to Coloumb's law, the total strength change, ΔS, along the pre-existing fault plane due to reservoir impoundment is given by (Bell and Nur, 1978):

$$\Delta S = \mu(\Delta\sigma_n - \Delta P) - \Delta\tau, \qquad (1a)$$

and

$$\Delta P = (\Delta P_u + \Delta P_{diff}), \qquad (1b)$$

where $\Delta\sigma_n$ and $\Delta\tau$ are the changes in normal and shear stresses, respectively, and μ is the coefficient of friction. The change in pore pressure, ΔP, occurs in two ways: instantly, in response to undrained loading, ΔP_u, in which the porous rock is compressed, yet fluids remain confined within it (e.g., Skempton, 1954); and after a time delay by diffusion of pore pressure ΔP_{diff} from the reservoir into the shallow crustal rocks. Negative values of ΔS signify weakening of the fault, while positive values imply strengthening. An increase in ΔP weakens the fault.

Neglecting nonlinear effects, the subsurface responds elastically to the reservoir loading by changing normal and shear stresses on a fault plane. An increase in normal stress strengthens the subsurface fault, while a change of shear stress may weaken or strengthen the fault depending on the orientation of the fault relative to the regional stress field. The instantaneous, or undrained change in strength, ΔS_u, occurs due to an elastic response to loading. It is given by

$$\Delta S_u = \mu(\Delta\sigma_n - \Delta P_u) - \Delta\tau. \qquad (1c)$$

Knowing the filling history, hypocentral locations and orientation of fault planes on which the earthquakes occurred, we can calculate $\Delta\sigma_n$, ΔP_u, and $\Delta\tau$, and thus, ΔS_u from equation (1c). Assuming the hydraulic diffusivity of the fractures, we can calculate ΔP_{diff}, and from equations (1b) and (1a), we can obtain the total change in strength, ΔS, at the hypocenter at the time of the earthquake.

We illustrate this technique with observations from Monticello Reservoir, South Carolina, where hypocentral data associated with the impoundment of the reservoir are available.

Initial Seismicity at Monticello Reservoir

Located in central South Carolina, Monticello Reservoir is the source of cooling and makeup water for the Virgil C. Summer Nuclear Station (Fig. 1). Filling of the reservoir started on 3 December 1977 and was completed on 8 February 1978 (Fig. 2). The reservoir has a surface area of 27 km^2 and a storage volume of 0.49 km^3 (Talwani and Acree, 1987).

Seismic monitoring started before the reservoir was impounded. A permanent three-component seismic station, JSC, located 3 km southeast of the reservoir, has been in operation since early November 1973. An additional four seismic stations (Fig. 1) were established by South Carolina Electric & Gas Company three months before the reservoir was impounded (Talwani and Acree, 1987). These five stations were used to locate subsequent seismicity. The earthquakes were located using the computer program HYPO71

(Lee and Lahr, 1972) and a five-layer velocity model developed for the RIS at Monticello Reservoir (Talwani and Acree, 1987).

The velocity model was developed by incorporating data from two sources. The shallow (<1 km) velocity structure was obtained from a velocity log in deep well no. 1 (Fig. 1). The deeper structure was obtained from two calibration shots in a shallow well (at depths of 20–30 m) located on the western shore of Monticello Reservoir (near cluster 3 in Fig. 1). The origin times of the blasts were obtained from a seismograph located near the shot point. Impulsive P- and S-wave arrivals were used to obtain V_P and V_S. The velocity model was tested using travel-time data and the earthquake location program HYPO71 (Lee and Lahr, 1972) to compare the computed locations of the blasts with their actual location. The two blasts were located within 100 and 50 m (epicentral distance) and 260 and 130 m (hypocentral distance) from the shot points. Talwani and Acree (1987) concluded that, conservatively, the epicentral and hypocentral accuracy of earthquakes located within the network was better than 200 and 500 m, respectively.

The solution quality ratings from HYPO71, A–D, of the hypocenters indicate the general reliability of the solution. Quality rating A indicates excellent epicenter and a good focal depth; B indicates good epicenter and fair depth; C indicates a fair epicenter and poor depth; and D indicates poor epicenter and poor depth. (For a quantitative explanation, see Lee and Lahr [1972].)

Earthquake activity began three weeks after the start of reservoir impoundment (Fig. 2). Within the first two months, through January 1978, 87 earthquakes were located with B and C qualities (Talwani and Acree, 1987).

The epicentral distance to the nearest station was less than 5 km (often less than 3 km), and the events were located by using eight or more phases including three or more S-wave phases. These parameters suggest that the hypocentral locations were accurate to better than 1 km, (see, e.g., Gomberg *et al.*, 1990). During filling there were minor changes in the V_P/V_S ratio (1.76 ± 0.02). The differences in computed distances due to differences in V_P/V_S ratio were less than 3%. For the farthest station with (S-P) equal to about 1 sec, the difference in calculated hypocentral distance is about ±200 m. Thus we conclude that the hypocentral locations are accurate enough to be used for stress calculations.

For stress calculations we used a subset of the data with location quality B, standard error of the epicenter (ERH) less than 1 km, standard error of the focal depth (ERZ) less than 1 km, and root mean square error of time residuals less than 0.1 sec. Fifty-three earthquakes satisfied these criteria (Table 1), of which 46 had ERH less than or equal to 500 m and 41 had ERZ less than or equal to 700 m. These 53 earthquakes occurred in or very close to the reservoir, and no earthquake was located in the deepest part of the reservoir (Fig. 1). Using a method detailed in the next section of this article, we calculated the total strength change, ΔS, at the time and hypocentral location of each earthquake. ΔS was obtained
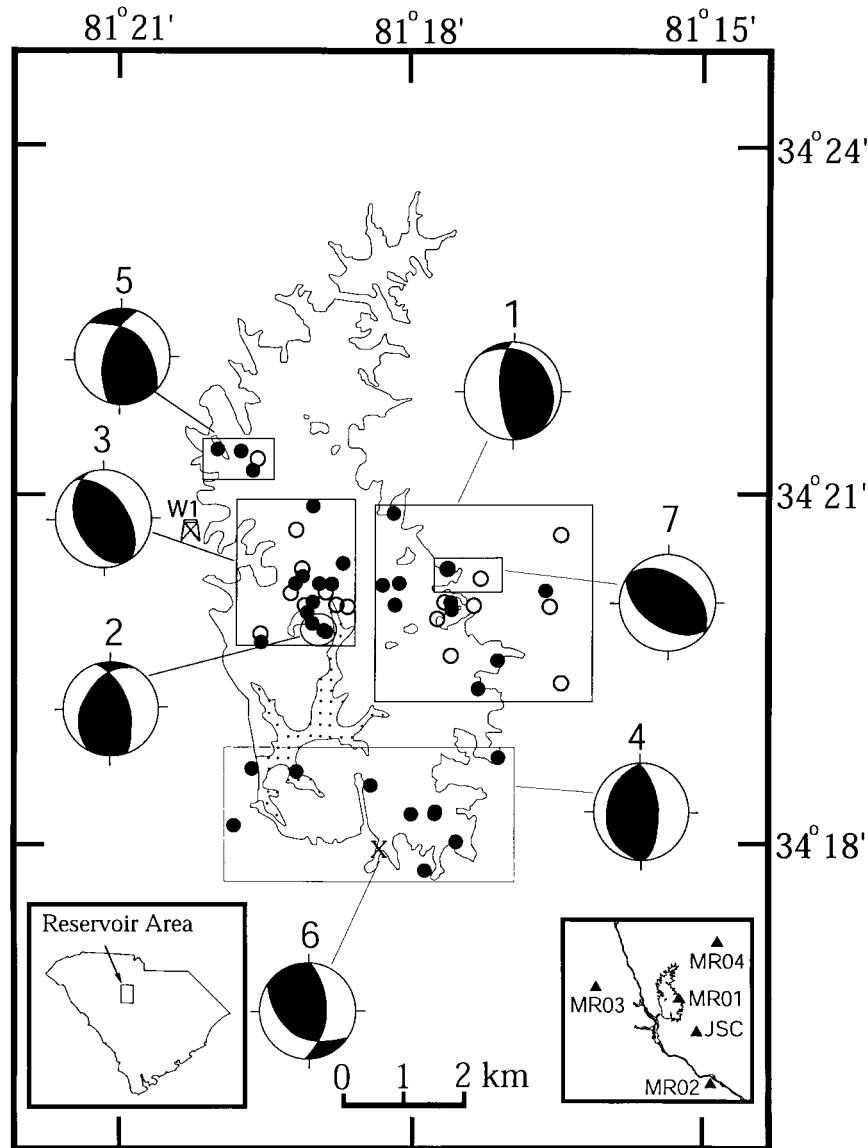
Figure 1.   Shows locations of initial seismicity to January 1978 at Monticello Reservoir. Insets show the location of the reservoir in south Carolina and the seismic stations used to locate the earthquakes. Open and solid circles show locations of earthquakes where the undrained effect due to impoundment of the reservoir resulted in weakening and strengthening, respectively. Boxed groups of epicenters and related fault-plane solutions for various locations are from Talwani and Acree (1987). X shows the location of the earthquake showing the largest strengthening. The stippled area shows the deepest part of the reservoir where no initial seismicity was observed. W1 shows the location of deep borehole 1.

by first calculating the undrained change in strength, ΔS_u, and then the change in pore pressure due to diffusion ΔP_{diff}.

Calculation of Stress and Strength Changes

Stress Changes due to the Undrained Effect

Boussinesq solutions (Jaeger and Cook, 1969) were used to calculate elastic stress changes caused by reservoir impoundment assuming a homogeneous medium. Stress changes were calculated at each hypocenter due to the water level in the reservoir at the time of the earthquake. The surface of reservoir was gridded into 55 grid blocks, each on a 1 km $\times$ 1 km scale on a 1:24,000 scale topographic map. The epicenters were then plotted on the topographic map. Each grid block that contained an earthquake was further divided into four 0.5 km $\times$ 0.5 km blocks. The total stress change at each hypocenter was obtained by summing the stress changes due to the water level rise in each grid block.
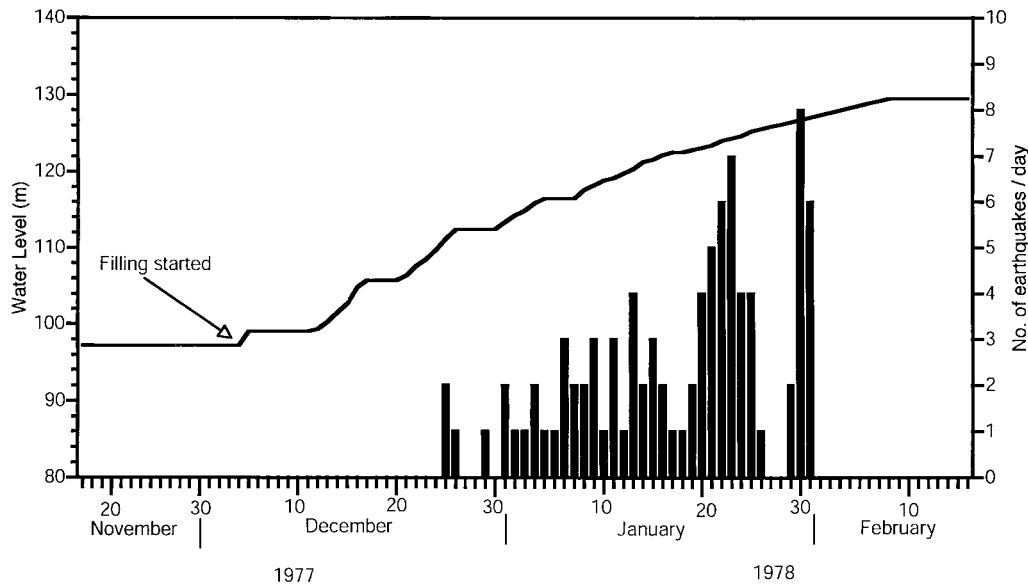
Figure 2.   Comparison of filling curve of Monticello Reservoir and initial seismicity to January 1978. Seismicity began about three weeks after the beginning of impoundment.

The sign convention used was positive for compression and negative for extension.

Figure 3a shows the coordinate system used in our calculations. The elastic stress changes at the hypocenter (*x, y, z*) caused by an average water level increase (Δh) over a surface area (A) within each grid (A $\leq$ 1 km²) due to reservoir impoundment were calculated using the following equations for a point load (Jaeger and Cook, 1969):

$$\sigma_{xx} = \frac{p}{2\pi}\left\{\frac{3x^2z}{r^5} + \frac{G(y^2+z^2)}{(\lambda+G)r^3(z+r)} - \frac{Gz}{(\lambda+G)r^3} - \frac{Gx^2}{(\lambda+G)r^2(z+r)^2}\right\},$$

$$\sigma_{yy} = \frac{p}{2\pi}\left\{\frac{3y^2z}{r^5} + \frac{G(x^2+z^2)}{(\lambda+G)r^3(z+r)} - \frac{Gz}{(\lambda+G)r^3} - \frac{Gy^2}{(\lambda+G)r^2(z+r)^2}\right\},$$

$$\sigma_{zz} = \frac{3pz^3}{2\pi r^5},$$

$$\tau_{yz} = \frac{3pyz^2}{2\pi r^5},$$

$$\tau_{xz} = \frac{3pxz^2}{2\pi r^5},$$

$$\tau_{xy} = \frac{p}{2\pi}\left\{\frac{3xyz}{r^5} - \frac{Gxy(z+2r)}{(\lambda+G)r^3(z+r)^2}\right\}, \qquad (2)$$

where $p = \rho g \Delta h A$,

$r = (x^2 + y^2 + z^2)^{1/2}$ is the distance from the hypocenter to the center of mass, σ_{xx}, σ_{yy}, and σ_{zz} are normal components, τ_{xy}, τ_{xz}, and τ_{yz} are shear components of the stress changes at the hypocenter, *p* is the weight increase of water due to the water level increase on the grid, ρ is the density of water, *g* is the acceleration due to gravity, *A* is the surface area of the part of the grid with water level increase and Δh is the average water level increase in the grid; λ and *G* are

Lamé constants. Based on the data for the shallow crust near Monticello Reservoir (V_P = 6.2 km/sec, V_P/VS = 1.76, and density of crustal rocks, ρ_R = 2.7 × 10³ kg/m³), we obtained λ = 3.77 × 10⁴ MPa and *G* = 3.37 × 10⁴ MPa.

The total stress changes $\sigma_{ii}(T)$ and $\tau_{ij}(T)$ were obtained by summing the contributions of each grid. These values were used in equations (3) and (4).

The pore pressure change due to the undrained effect (Skempton, 1954) is

$$\Delta P_u = B\bar{\sigma}, \qquad (3)$$

where the average normal stress change is $\bar{\sigma} = \sigma_{ii}(T)/3$, and *B* is Skempton's coefficient; we assume *B* = 0.7 (Talwani *et al.*, 1999).

To calculate the stresses we needed to identify the fault planes on which the hypocenters were located. We used extensive fault-plane solution and borehole and surface data wherein the geometries of various fractures had been determined. Talwani and Acree (1987) obtained 22 composite fault-plane solutions for various clusters of seismicity, and all of them showed reversed faulting. These varied according to the depth of the hypocenter and according to their association with the lithology in the area—migmatites, granites, or gneisses.

The poles of these fault planes were compared with those of the fractures encountered in the two deep holes (Seeburger and Zoback, 1982) and those encountered in different lithologies during construction of the Virgil C. Summer Nuclear Station (South Carolina Electric & Gas Company, 1977). Excellent agreement between the set of poles of fractures with those of the nodal planes allowed us to determine the strike and dip of the focal planes as a function of their location, depth, and geologic association (Talwani

Table 1
Focal Parameters of the Earthquakes Used for Stress Calculations

Event No.	Date (mmddyy)	Origin (hr:min:sec)	Lat N (34° min)	Long W (81° min)	Depth (km)	M_L	RMS (sec)	ERH (km)	ERZ (km)
1	122577	12 08 27.18	20.29	18.39	1.41	1.32	0.04	0.20	0.30
2	122677	04 49 44.89	19.68	19.55	1.67	2.33	0.06	0.30	0.60
3	122977	12 03 11.34	20.01	19.14	0.41	1.64	0.06	0.20	0.00
4	123177	22 39 55.89	20.01	17.66	1.00	1.18	0.05	0.20	0.30
5	123177	23 38 08.22	19.90	17.84	0.29	0.82	0.05	0.20	0.30
6	010378	01 24 06.56	20.21	18.17	1.43	1.32	0.03	0.20	0.20
7	010378	22 12 46.53	20.21	16.63	0.58	1.44	0.05	0.30	0.60
8	010478	08 26 19.88	19.99	19.17	1.64	1.32	0.06	0.40	0.80
9	010678	14 44 22.73	19.86	19.10	1.07	1.64	0.07	0.30	0.90
10	010678	21 03 08.57	20.87	19.07	3.55	1.54	0.05	0.30	0.50
11	010678	22 05 07.25	20.15	19.32	0.39	1.80	0.07	0.20	0.60
12	010778	06 59 19.18	20.01	17.62	2.44	1.18	0.03	0.20	0.40
13	010878	22 12 46.53	20.16	18.98	0.67	1.02	0.05	0.20	0.40
14	010878	22 12 53.57	20.31	19.20	0.28	0.00	0.07	0.30	0.90
15	010978	03 58 11.14	20.19	18.88	1.50	1.02	0.07	0.40	0.60
16	010978	12 42 13.63	20.28	19.18	0.25	1.44	0.05	0.00	0.90
17	011078	07 48 40.19	18.74	17.16	2.57	1.09	0.09	0.60	0.90
18	011178	16 28 24.20	20.28	17.35	0.45	2.16	0.04	0.20	0.30
19	011278	04 24 35.54	20.01	18.27	2.02	1.54	0.06	0.40	0.30
20	011378	03 13 49.13	19.80	18.96	1.84	1.32	0.08	0.40	0.70
21	011378	03 59 24.95	20.01	19.09	1.10	1.18	0.04	0.20	0.60
22	011378	22 32 40.80	18.25	17.84	1.78	0.95	0.03	0.20	0.50
23	011478	08 58 18.24	18.47	18.49	2.71	0.95	0.07	0.60	0.70
24	011578	01 18 49.92	20.37	18.76	0.70	1.54	0.05	0.30	0.7
25	011678	12 10 50.62	19.61	17.61	0.49	0.91	0.04	0.60	0.70
26	011778	16 46 54.54	19.36	16.50	0.57	1.18	0.05	0.30	0.90
27	011878	05 14 51.21	19.33	17.34	1.17	1.80	0.08	0.40	0.60
28	011978	14 45 39.15	20.01	17.38	1.00	1.44	0.09	0.50	0.50
29	011978	15 25 11.80	20.18	16.66	3.59	1.32	0.07	0.40	0.40
30	012078	16 33 35.50	20.41	17.72	0.53	0.24	0.03	0.70	0.70
31	012178	06 37 51.36	18.57	19.27	4.31	0.21	0.07	0.30	0.70
32	012178	09 25 51.42	19.56	17.13	1.81	1.46	0.07	0.30	0.60
33	012178	14 18 24.63	20.79	18.84	2.18	1.44	0.07	0.30	0.50
34	012278	01 08 09.28	20.01	18.84	0.05	1.37	0.04	0.30	0.50
35	012278	01 36 37.18	19.77	19.59	0.28	0.00	0.08	0.30	0.70
36	012278	03 13 13.38	20.68	19.26	0.14	1.44	0.07	0.30	0.80
37	012278	23 12 28.54	19.82	18.94	1.20	1.44	0.06	0.30	0.70
38	012378	06 41 57.17	20.01	17.63	1.00	1.24	0.05	0.30	0.30
39	012378	13 19 45.06	18.25	17.84	1.76	0.00	0.06	0.20	0.70
40	012478	00 26 11.27	20.03	18.70	0.30	1.12	0.09	0.30	0.50
41	012578	08 29 38.70	18.00	17.60	1.91	2.77	0.06	0.30	0.70
42	012578	09 29 26.39	17.79	17.94	1.82	2.37	0.05	0.30	0.80
43	012978	07 14 12.38	20.22	19.27	1.18	1.06	0.05	0.30	0.80
44	012978	17 32 42.29	18.59	19.76	1.83	1.44	0.08	0.30	0.90
45	013078	01 36 13.12	21.19	19.75	3.64	0.87	0.06	0.40	0.70
46	013078	03 24 59.32	21.36	20.12	5.24	1.24	0.07	0.60	0.90
47	013078	03 54 29.12	21.34	19.87	5.41	0.00	0.07	0.60	0.70
48	013078	04 57 51.88	20.19	18.99	2.50	0.95	0.06	0.40	0.40
49	013078	08 21 43.03	21.27	19.70	0.43	1.45	0.04	0.20	0.70
50	013178	03 32 27.63	18.25	18.05	1.84	1.18	0.06	0.40	0.70
51	013178	03 15 25.52	17.93	18.40	0.67	1.62	0.05	0.20	0.60
52	013178	09 56 32.73	18.13	19.93	1.98	0.00	0.05	0.20	0.90
53	013178	16 23 14.79	20.62	16.49	1.96	0.44	0.06	0.40	0.60

and Acree, 1987). The fault-plane solutions for each of the 53 earthquakes in this study were inferred according to the hypocentral locations and comparison with the fault-plane solutions of Talwani and Acree (1987). Seven fault-plane solutions were chosen for these earthquakes (Table 2, Fig.

1). Fault-plane solutions 1 and 5 are for earthquakes whose hypocenters are in granitic rocks, 2 for earthquakes in gneisses, 4 are for earthquakes in the southern part of the reservoir in migmatites, granites, and gneisses, and 3 and 7 are for earthquakes in migmatites. The single event X, as-
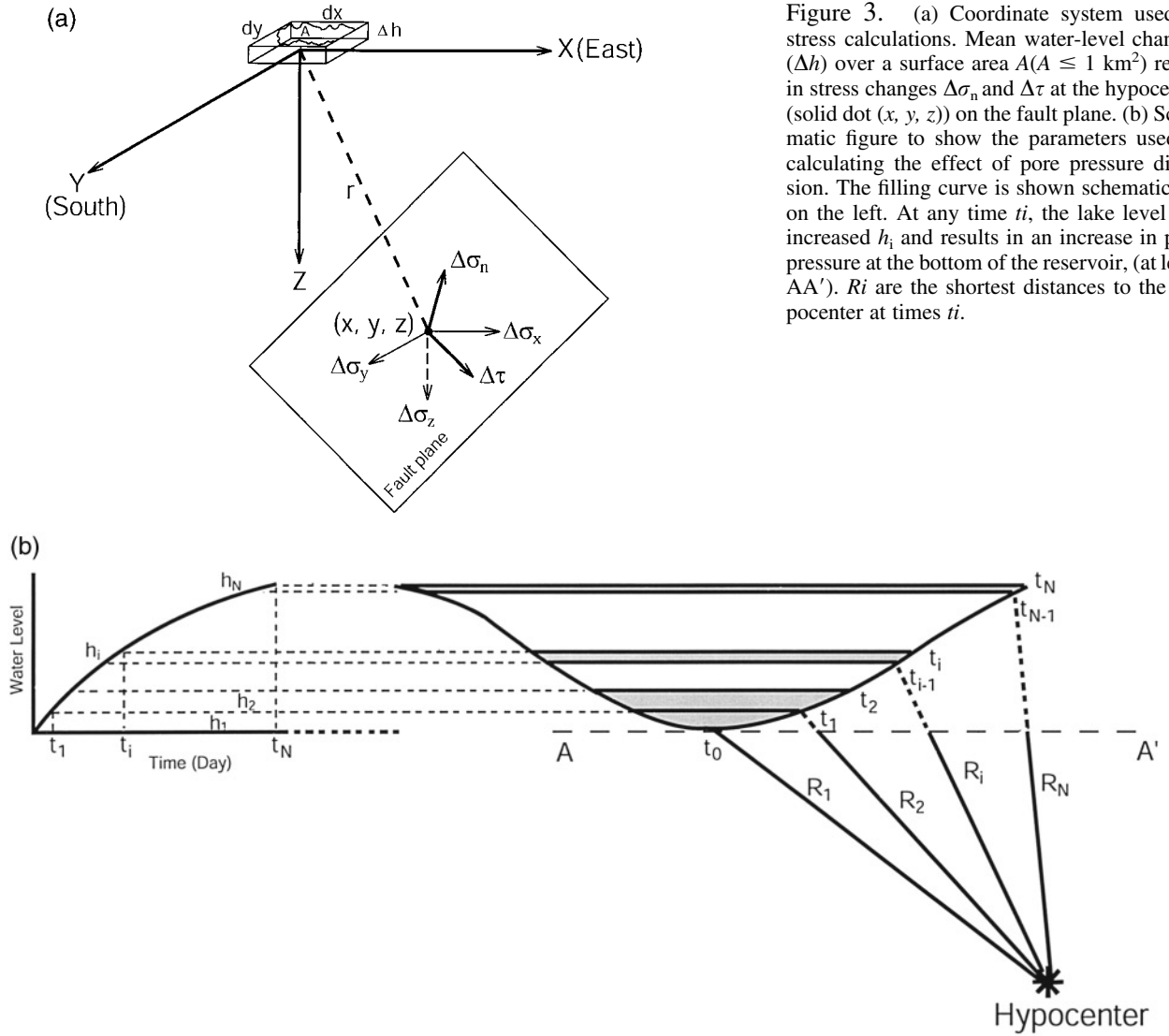
Figure 3. (a) Coordinate system used in stress calculations. Mean water-level changes (Δh) over a surface area $A(A \leq 1 \ km^2$) result in stress changes $\Delta\sigma_n$ and $\Delta\tau$ at the hypocenter (solid dot (x, y, z)) on the fault plane. (b) Schematic figure to show the parameters used in calculating the effect of pore pressure diffusion. The filling curve is shown schematically on the left. At any time t_i, the lake level has increased h_i and results in an increase in pore pressure at the bottom of the reservoir, (at level AA'). Ri are the shortest distances to the hypocenter at times t_i.

Table 2
Attitudes of the Nodal Planes

Solution Number	Fault Plane		Auxiliary Plane	
	Strike (°)	Dip (°)	Strike (°)	Dip (°)
1	N02W	69W	N38W	24E
2	N17W	60E	N28E	40W
3	N26W	43W	N35W	50NE
4	N03E	60E	N56W	48W
5	N18E	60W	N41W	48E
6	N06W	62E	NS	28W
7	N59W	48SW	N52W	42NE

sociated with fault-plane solution 6, was shallow (<1 km) and located in migmatite, whereas the nearby events associated with fault-plane solution 4 were deeper than 1 km.

Next, for each earthquake, all stress components were projected on each of the inferred fault planes. The total *x, y,* and *z* components of the stress change across the fault plane are given by (Jaeger and Cook, 1969)

$$\Delta\sigma_x(T) = l\sigma_{xx}(T) + m\tau_{yx}(T) + n\tau_{zx}(T),$$
$$\Delta\sigma_y(T) = m\sigma_{yy}(T) + l\tau_{xy}(T) + n\tau_{zy}(T), \qquad (4)$$
$$\Delta\sigma_z(T) = n\sigma_{zz}(T) + m\tau_{yz}(T) + l\tau_{xz}(T),$$

where *l, m, n* are the direction cosines of the normals to the fault plane. The normal and the shear stresses across the fault plane (Fig. 3a) are given by (Jaeger and Cook, 1969)

$$\Delta\sigma_n = l\Delta\sigma_x(T) + m\Delta\sigma_y(T) + n\Delta\sigma_z(T), \qquad (5a)$$

and

$$\Delta\tau = \pm\sqrt{(\Delta\sigma_x(T)^2 + \Delta\sigma_y(T)^2 + \Delta\sigma_z(T)^2) - \Delta\sigma_n^2}, \qquad (5b)$$

where $\Delta\tau$ is positive when the shear stress favors faulting. The calculated values for $\Delta\sigma_n$ and $\Delta\tau$ for each event are listed in Table 3.

Table 3
Results of Calculation of Strength Changes

Event No.	Water Level (m)	ΔP_u (MPa)	FPS No.	$\Delta\sigma_n$ (MPa)	$\Delta\tau$ (MPa)	ΔS_u (MPa)	$C = 0.5$ m²/sec		$C = 2$ m²/sec		$C = 5$ m²/sec	
							ΔP_{diff} (MPa)	ΔS (MPa)	ΔP_{diff} (MPa)	ΔS (MPa)	ΔP_{diff} (MPa)	ΔS (MPa)
1	14.34	0.014	3	0.013	−0.026	0.025	0.014	0.014	0.048	−0.011	0.0772	−0.029
2	14.34	0.014	3	0.012	−0.024	0.023	0.010	0.015	0.043	−0.010	0.070	−0.029
3	14.64	0.021	3	−0.011	0.016	−0.040	0.081	−0.101	0.111	−0.123	0.123	−0.132
4	15.86	0.009	1	0.003	0.010	−0.015	0.038	−0.043	0.083	−0.077	0.105	−0.093
5	15.86	0.049	1	0.005	0.071	−0.104	0.085	−0.168	0.114	−0.190	0.126	−0.199
6	18.30	0.017	1	0.023	−0.033	0.037	0.031	0.014	0.081	−0.024	0.110	−0.045
7	18.30	0.006	1	−0.001	0.002	−0.007	0.032	−0.031	0.084	−0.069	0.112	−0.091
8	18.30	0.022	3	0.044	−0.050	0.067	0.022	0.050	0.071	0.014	0.102	−0.010
9	18.61	0.033	2	0.095	−0.070	0.117	0.058	0.074	0.108	0.036	0.132	0.018
10	18.61	0.005	3	0.008	−0.011	0.014	0.001	0.013	0.025	−0.005	0.058	−0.030
11	18.61	0.022	3	0.012	0.024	−0.032	0.111	−0.115	0.143	−0.139	0.155	−0.149
12	18.91	0.012	1	0.038	−0.024	0.044	0.010	0.036	0.054	0.003	0.090	−0.023
13	19.52	0.026	3	0.023	0.030	−0.031	0.093	−0.101	0.135	−0.132	0.153	−0.146
14	19.52	0.034	3	0.038	−0.039	0.041	0.134	−0.060	0.160	−0.079	0.169	−0.086
15	19.83	0.028	3	0.036	−0.056	0.062	0.043	0.030	0.098	−0.011	0.127	−0.033
16	20.13	0.035	3	0.039	−0.040	0.043	0.152	−0.071	0.172	−0.086	0.179	−0.091
17	20.74	0.011	4	0.049	−0.012	0.040	0.010	0.033	0.056	−0.002	0.093	−0.030
18	21.05	0.012	7	0.000	0.005	−0.014	0.088	−0.079	0.140	−0.119	0.163	−0.136
19	21.35	0.022	1	0.044	−0.043	0.060	0.026	0.040	0.083	−0.003	0.119	−0.030
20	21.96	0.027	2	0.083	−0.058	0.100	0.033	0.076	0.093	0.031	0.129	0.004
21	21.96	0.035	3	0.020	−0.052	0.040	0.077	−0.017	0.132	−0.059	0.159	−0.079
22	22.88	0.018	4	0.065	−0.028	0.064	0.036	0.036	0.096	−0.009	0.132	−0.035
23	22.88	0.019	4	0.073	−0.031	0.072	0.012	0.063	0.062	0.025	0.103	−0.005
24	23.49	0.048	3	0.030	−0.068	0.054	0.123	−0.038	0.168	−0.071	0.187	−0.086
25	24.10	0.037	1	0.026	0.040	−0.049	0.150	−0.161	0.187	−0.189	0.202	−0.200
26	24.10	0.013	1	0.002	0.010	−0.019	0.115	−0.105	0.169	−0.146	0.192	−0.163
27	24.40	0.025	1	0.028	−0.043	0.045	0.080	−0.015	0.144	−0.063	0.175	−0.086
28	24.71	0.019	1	0.008	0.021	−0.029	0.084	−0.092	0.151	−0.143	0.183	−0.166
29	24.71	0.010	1	0.015	−0.023	0.027	0.003	0.025	0.039	−0.003	0.083	−0.036
30	25.01	0.031	7	0.013	−0.036	0.021	0.152	−0.092	0.194	−0.123	0.211	−0.136
31	25.32	0.011	4	0.036	−0.022	0.041	0.002	0.040	0.035	0.015	0.079	−0.019
32	25.32	0.018	1	0.020	−0.032	0.033	0.047	−0.002	0.118	−0.055	0.158	−0.085
33	25.32	0.017	1	0.030	−0.037	0.046	0.026	0.027	0.095	−0.025	0.139	−0.058
34	25.62	0.013	3	0.019	0.021	−0.017	0.231	−0.190	0.239	−0.196	0.241	−0.198
35	25.62	0.035	3	0.078	0.055	−0.022	0.185	−0.161	0.215	−0.183	0.226	−0.192
36	25.62	0.042	3	0.005	0.041	−0.069	0.220	−0.234	0.233	−0.244	0.238	−0.248
37	25.93	0.050	2	0.042	−0.089	0.083	0.094	0.012	0.158	−0.036	0.188	−0.058
38	25.93	0.026	1	0.016	0.032	−0.039	0.106	−0.119	0.169	−0.166	0.197	−0.187
39	26.23	0.022	4	0.077	−0.035	0.076	0.057	0.034	0.129	−0.020	0.167	−0.049
40	26.84	0.068	3	0.035	0.086	−0.111	0.198	−0.259	0.229	−0.282	0.240	−0.291
41	27.76	0.015	4	0.051	−0.026	0.053	0.048	0.017	0.121	−0.038	0.162	−0.068
42	27.76	0.014	6	0.038	−0.029	0.047	0.048	0.011	0.124	−0.046	0.166	−0.078
43	28.37	0.052	3	0.078	−0.104	0.123	0.113	0.039	0.184	−0.015	0.217	−0.040
44	28.67	0.028	4	0.103	−0.038	0.095	0.064	0.047	0.143	−0.013	0.187	−0.045
45	28.98	0.012	5	0.013	−0.023	0.024	0.008	0.018	0.066	−0.025	0.120	−0.066
46	28.98	0.008	5	0.011	−0.017	0.019	0.001	0.019	0.029	−0.002	0.077	−0.038
47	28.98	0.007	5	0.009	−0.016	0.018	0.001	0.017	0.026	−0.002	0.073	−0.037
48	28.98	0.025	3	0.027	−0.050	0.051	0.033	0.027	0.110	−0.031	0.161	−0.069
49	28.98	0.020	5	0.011	0.006	−0.012	0.178	−0.146	0.230	−0.185	0.250	−0.200
50	29.28	0.030	4	0.106	−0.048	0.105	0.068	0.054	0.149	−0.007	0.193	−0.040
51	29.28	0.082	4	0.223	−0.158	0.264	0.179	0.129	0.230	0.091	0.251	0.075
52	29.28	0.018	4	0.060	−0.032	0.063	0.055	0.022	0.136	−0.039	0.183	−0.074
53	29.28	0.008	1	−0.001	0.002	−0.008	0.019	−0.023	0.094	−0.079	0.150	−0.121

The first two columns identify the event number and lake level at the time of the earthquake. Column 3 was obtained from equations (2) and (3). The fault-plane-solution number corresponds to Table 2. Columns 5, 6, and 7 were obtained from Equations (4), (5) and (1c). ΔP_{diff} was calculated for three values of C from equation 6 (columns 8, 10, and 12) and the corresponding changes in total strength from equation 1a (columns 9, 11, and 13).

Pore Pressure Increase due to Diffusion, ΔP_{diff}

Impoundment of Monticello Reservoir was achieved by pumping water from a downstream reservoir. The water-level curve from the start of pumping to the end of January 1978 is shown in Figure 2. The water-level rise results in increasing pore pressures at the bottom of the reservoir. These additional pore pressures diffuse to the hypocenter according to the pore pressure diffusion equation. Because the increase in pore pressure corresponding to increase in lake level, h_i, is the same at any level within the reservoir, to calculate ΔP_{diff}, we took the shortest distance to the hypocenter from the reservoir, R_i, (Fig. 3b). With the filling of hitherto unsubmerged areas, the location of surface area under water increases, and the shortest distance to the hypocenter, R_i decreases (Fig. 3b).

Figure 3b illustrates the parameters used in the calculation of ΔP_{diff} at the hypocenter at the time of the earthquake. The filling curve is shown schematically on the left, where h_i represents the daily water-level increase. For example, at time t_1 the water level had increased by h_1 over the initial level, and at time t_2, the water level had gone up h_2 above the level at time t_1. Water levels at different times, t_i, are shown on the right. AA′ represents the elevation of the bottom of the reservoir, and R_i are the shortest distances from the hypocenter to the filled part of the reservoir at times t_i. The distances, R_i, are of the order of a few kilometers, and as the total height of the fully impounded reservoir is about 30 m, we approximate the distances R_i with distances from the hypocenter up to the level AA′. The increase in pore pressure at the level AA′ at time t_1 is due to a head of water with height h_1. It diffuses to the hypocenter at a distance R_1 away, where it reaches after some time delay. At time t_2 there is an additional pore pressure due to the added height of the water, h_2. It too diffuses to the hypocenter, but now the shortest distance is R_2. So after some time delay, the pore pressure at the hypocenter further increases due to the increased head at t_2. Therefore, the increase in pore pressure at the hypocenter at any time is the sum of the increases in pore pressures (by diffusion) corresponding to earlier incremental increases in the lake level.

Both surface and borehole data (South Carolina Electric & Gas Company, 1977; Seeburger and Zoback, 1982) attest to the presence of isolated regions of well developed fractures in the crystalline rocks. These fractures follow well developed foliation planes. Based on our experience at Bad Creek Reservoir, in similar metamorphic crystalline rocks (Talwani *et al.*, 1999) and at other locations, (e.g., the KTB hole) (Kessels and Kück, 1995), long-term hydraulic behavior of inclined plane fractures can be sufficiently accurately calculated by using a one-dimensional model.

The cumulative pore pressure increase at the hypocenter at the time of the earthquake was calculated using the solution of the one-dimensional radial diffusion equation modified from Rajendran and Talwani (1992):

$$\Delta P_{\text{diff}} = \sum_{i=1}^{i=N} \left(1 - \text{erf} \left(\frac{R_i}{2\sqrt{C \Delta t_i}} \right) \right) (\Delta P_i), \qquad (6)$$

where C is the hydraulic diffusivity, and for various cases of RIS, it lies between 0.1 and 10 m^2/sec (Talwani and Acree, 1984; Talwani and Chen, 1998); $\Delta P_i = \rho g h_i$ and h_i is water level increase on the ith day, Δt_i is the time elapsed between the time of that water level increase and the time of earthquake, N is the total number of days between the start of reservoir impoundment and the time of earthquake.

Strength Change

The undrained change in strength, ΔS_u, and the total change in strength, ΔS, were calculated from equations (1c) and (1a), respectively. The calculations involved the following steps. The undrained (instantaneous) change in the stress at the hypocenter was due to the load of the whole reservoir. The stress changes $\Delta \sigma_n$ and $\Delta \tau$ at the hypocenter were obtained by dividing the reservoir into grid blocks and adding the contribution of each block to $\Delta \sigma_n$ and $\Delta \tau$ at the hypocenter (equations 5a, b). The instantaneous undrained pore pressure change, ΔP_u at the hypocenter in response to the load was calculated from equation (3). These values of $\Delta \sigma_n$ and $\Delta \tau$ and ΔP_u were used in equation (1c) to obtain ΔS_u. Following Byerlee (1978), $\mu = 0.75$ was assumed.

The change in pore pressure at the hypocenter by diffusion, ΔP_{diff}, was the delayed response to the increases in pore pressure at the bottom of the reservoir due to the increasing lake levels, h_i. In calculating ΔP_{diff} (equation 6), the hydraulic diffusivity was unknown. We calculated ΔP_{diff} for nine different values of C ranging between 0.1 m^2/sec and 10 m^2/sec. This range covers the observed range of C for cases of induced seismicity (Talwani and Acree, 1984; Talwani and Chen, 1998). Of these nine sets of calculations we show the results obtained by using $C = 0.5$ m^2/sec, 2 m^2/sec, and 5 m^2/sec. The calculated pore pressure change due to diffusion at the time of the earthquake ΔP_{diff} (from equation 6) was added to the undrained change in pore pressure, ΔP_u, from equation (3) to obtain the total change in pore pressure, ΔP (equation 1b), which was then used in equation (1a) to obtain the total (combined) change in strength ΔS.

Sample Calculation

We illustrate our methodology with a sample calculation of ΔS_u and ΔS for event 20, which occurred on 13 January 1978 at 03 hr 13 min 49.13 sec. At that time the lake level had risen about 22 m since impoundment started, and the water level increased in 34 of the grid blocks. To obtain the stress components for each grid block, we substituted the mean water-level increase Δh, surface area A, and hypocentral distance r in equation (2) (Appendix I). The total contribution of all the grids gave $\sigma_{xx}(T) = 0.007$ MPa, $\sigma_{yy}(T) = 0.020$ MPa, $\sigma_{zz}(T) = 0.091$ MPa, $\tau_{xy}(T) = 0.016$ MPa,

$\tau_{xz}(T) = 0.032$ MPa, and $\tau_{yz}(T) = 0.045$ MPa. Assuming $B = 0.7$, from equation (3) we then obtain $\Delta P_u = 0.027$ MPa (Table 3).

We next calculated the undrained elastic loading effect at the hypocenter for this event on the specific fault plane. Based on its hypocentral location, this event was inferred to be associated with fault-plane solution 2, and the inferred fault plane had a strike of N17°W and a dip of 60°E (Table 2). The direction cosines of the fault plane are $l = 0.47$, $m = -0.15$, and $n = 0.87$. From equations 4, 5a, and 5b, we get $\Delta\sigma_n = 0.083$ MPa and $\Delta\tau = -0.058$ MPa. Since the increase in vertical normal stress was much greater than that in the horizontal stresses (Appendix I), the increase of shear stress was not in favor of failure, so we assigned the change in shear stress $\Delta\tau$ (equation 5b) a negative value. Assuming $\mu = 0.75$ (Byerlee, 1978), from equation (1c), we get $\Delta S_u = 0.100$ MPa (Table 3).

Finally, we determined the pore pressure changes at the time and location of the event due to diffusion of pore pressure. The time delay between the start of impoundment and the time of the earthquake is 41 days, of which there were 26 days when there was an increase in the water level ($h_i > 0$). The pore pressure increase at the hypocenter of the event due to each of these 26 increases was calculated using equation (6) for nine different hydraulic diffusivity values, and the results for three values are shown (Appendix II). The sum of all 26 step increases for different values of C were used to get ΔP_{diff} (Table 3). The total change due to both the undrained effect and drained effect, ΔS, for each value of C was calculated using Coulomb's law, equation (1a), and the results are listed in Table 3.

Results

Figure 4 compares the instantaneous (or undrained) changes in strength associated with reservoir impoundment, ΔS_u, with total changes in strength due to the combined undrained and diffusion effects, ΔS. Of the 53 earthquakes undrained, elastic loading resulted in weakening for 17, of which 16 had a depth less than or equal to 1 km (Fig. 4a). Of these 17, only 7 were below the spreading lake waters at the time of the earthquakes. Except for three very shallow events with z less than 400 m, the magnitude of weakening is less than or equal to 0.05 MPa. Of the 36 events that showed strengthening due to loading, 31 were ≥ 1 km deep. The magnitude of strengthening is about 0.25 MPa or less. Thus, seismicity associated with the undrained elastic loading effect of impoundment can at best account for only the shallow (<1 km deep) earthquakes at Monticello Reservoir. An absence of initial seismicity below the deepest part of the Monticello Reservoir (Fig. 1) further attests to the strengthening effect of loading. (Earthquakes beneath the deepest part of the reservoir did not occur until 1985 [Talwani and Acree, 1987]).

We calculated the hydrostatic restoring stress due to flexure caused by the loading of the reservoir, σ_w, which is given by

$$\sigma_w = (\rho_R - \rho)gW_i, \qquad (7)$$

where ρ_R and ρ are the densities of rock and water, and W_i is the flexure corresponding to the load of water (Turcotte and Schubert, 1982). For Monticello Reservoir, the maximum flexure corresponding to about 30 m of water is 0.01 m, and the calculated stress due to flexure below the deepest part of the reservoir is 0.0002 MPa. It is even lower outside the reservoir. Thus the stress changes due to flexure do not contribute to the seismicity. We thus conclude that an increase in pore pressure by diffusion accounts for the greater bulk of observed seismicity.

Such an effect is illustrated by calculating the total changes in strength, ΔS, that incorporate both the undrained elastic loading and pore pressure diffusion effects for three values of hydraulic diffusivity (Fig. 4b–d). Weakening increases with an increase in hydraulic diffusivity, C. For $C = 5$ m²/sec, weakening predominates. This value is at the high end of seismogenic diffusivity (0.1 to 10 m²/sec) found to be characteristic of cases of induced seismicity (Talwani and Chen, 1998). The maximum weakening, about 0.3 MPa, is associated with a shallow event ($z \approx 0.4$ km) and 0.1 MPa for the deeper events ($z \geq 1$ km). We can estimate the permeability, k, of the fractures from the inferred value of hydraulic diffusivity, C, following Bodvarsson (1970):

$$k = Cv[\phi\beta_f + (1-\phi)\beta_r].$$

Assuming a porosity, $\phi = 3 \times 10^{-3}$; viscosity of water at hypocenter, $v = 0.5 \times 10^{-3}$ Pa (s) (Weast, 1987); compressibility of fluid, $\beta_f = 4.6 \times 10^{-10}$ Pa⁻¹, and compressibility of rock, $\beta_r = 2 \times 10^{-11}$ Pa⁻¹ (Talwani and Acree, 1984; Talwani et al., 1999), a diffusivity value, $C = 5$ m²/sec corresponds to a permeability, $k = 5 \times 10^{-14}$ m² (50 mD).

Since most of the seismicity was shallow and at relatively small hypocentral distances from the reservoir, we tested the effect of location accuracy on our results. We calculated ΔS_u for the given depth, Z, and for $Z \pm$ ERZ for all 53 events. The changes in ΔS_u varied from less than 0.005 MPa to 0.06 MPa. We also calculated changes in ΔS_u for epicentral inaccuracies of five representative events by perturbing the location by ERH in north, south, east, and west directions. The changes in ΔS_u varied from about 0.02 MPa to 0.06 MPa. But, importantly, these calculations showed that at most of the hypocenters, impoundment of the reservoir led to strengthening, and only after there was an increase in pore pressure by diffusion did we get weakening. In other words, inaccuracies in the hypocentral locations did not alter the main observation; the effect of undrained elastic loading was strengthening at most hypocentral locations.
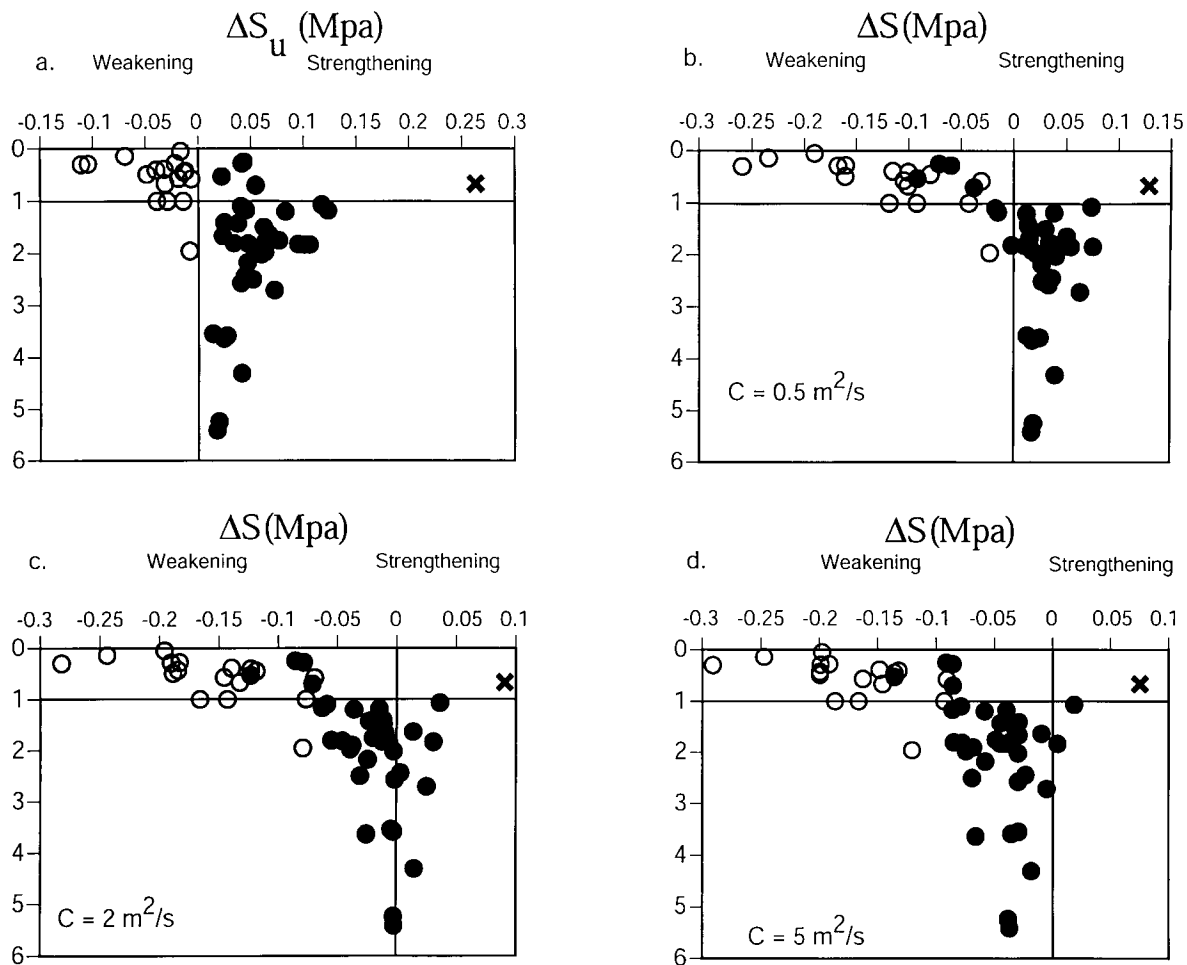
Figure 4. Comparison of (a) undrained strength changes, ΔS_u (Fig. 4a), with coupled poroelastic strength changes, ΔS for $C =$ (b) 0.5, (c) 2, and (d) 5 m²/sec. Open circles are events that show weakening due to undrained effect, whose locations are shown in Figure 1. These events may or may not have been triggered by elastic loading and the resultant increase in undrained pore pressure (ΔS_u); the faults on which they occurred were subsequently further weakened by the process of pore pressure diffusion. Weakening for all events increases with increasing diffusivity, C. $\times$ shows the earthquake with largest strengthening.

Discussion and Conclusions

Earlier studies investigated elastic (undrained) stress changes due to reservoir impoundment at Lake Kariba (Gough and Gough, 1970) and at Lake Oroville (Beck, 1976). In both studies, the authors calculated only the elastic stress changes and not the changes in pore pressure due to Skempton's effect. In their theoretical analysis of stress and strength changes due to reservoir impoundment, Bell and Nur (1978) considered both elastic stress and pore pressure changes due to diffusion. They found that the magnitude of strength change due to reservoir impoundment varied with assumed permeability values and the location of permeability contrast. In their heuristic study, Simpson *et al.* (1988) considered both elastic (undrained) and diffusion effects to

explain RIS. They ascribed initial seismicity at some shallow reservoirs, including the Monticello Reservoir, to the elastic (undrained) effect only.

The installation of a seismic network prior to impoundment and detailed complementary geological, borehole, and geophysical studies at Monticello Reservoir (Talwani and Acree, 1987) provided a unique data set to study the nature of the initial seismicity that followed impoundment. The development of a five-layer velocity model ensured accurate hypocentral locations. Using detailed information regarding filling history, focal mechanisms, and geology of the area, we calculated changes in strength ΔS_u and ΔS at the hypocenters for 53 well-located events. Our results can be summarized as follows:

1. Strength changes less than or equal to 0.1 MPa are enough to trigger RIS, which indicates that a large part of the crust beneath the reservoir area was in a state near critical failure before the reservoir was impounded. Our observation supports the suggestion of self-organized criticality, which claims that large parts of crust are very near the state of critical failure, so that small outside stress perturbations can trigger failure (Grasso and Sornette, 1998).
2. Changes in the undrained stress due to the combination of elastic loading and the concurrent increase in pore pressure due to this load on the undrained crustal rocks, can explain, at best, a small fraction of the initial seismicity.
3. The vast bulk of Reservoir Induced Seismicity at Monticello Reservoir is primarily associated with the diffusion of pore pressure.
4. The inferred diffusivity values, $C = 5\,\mathrm{m^2/sec}$, correspond to permeability, $k = 5 \times 10^{-14}\,\mathrm{m^2}$ (50 mD). These values are in agreement with an earlier estimate of permeability for Monticello Reservoir (Talwani and Acree, 1984) and with the inferred range of seismogenic permeability (Talwani and Chen, 1998).

Acknowledgments

References

Beck, J. L. (1976). Weight-induced stresses and the recent seismicity at Lake Oroville, California, *Bull. Seism. Soc. Am.* **66,** 1121–1131.

Bell, M. L., and A. Nur (1978). Strength changes due to reservoir-induced pore pressure and application to Lake Oroville, *J. Geophys. Res.* **83,** 4469–4483.

Bodvarsson, G. (1970). Confined fluids as strain meters, *J. Geophys. Res.* **75,** 2711–2718.

Byerlee, J. (1978). Friction of rocks, *Pageoph* **122,** 947–965.

Fletcher, J. B. (1982). A comparison between the tectonic stress measured *in situ* and stress parameters from induced seismicity at Monticello Reservoir, South Carolina, *J. Geophys. Res.* **87,** 6931–6944.

Gibowicz, S. J., and A. Kijko (1994). *An Introduction to Mining Seismology*, Academic Press, San Diego, 399 pp.

Gomberg, J. S., K. M. Shedlock, and W. Roecker (1990). The effect of S-wave times on the accuracy of hypocenter estimation, *Bull. Seism. Soc. Am.* **80,** 1605–1628.

Gough, D. I., and W. I. Gough (1970). Load-induced earthquakes at Lake Kariba. II, *Geophys. J. R. Astr. Soc.* **21,** 79–101.

Grasso, J.-D., and D. Sornette (1998). Testing self-organized criticality by induced seismicity, *J. Geophys. Res.* **103,** 29,965–29,999.

Hutchenson, K. D. (1982). Source studies of reservoir induced earthquakes at Monticello Reservoir, South Carolina, *M.S. Thesis*, University of South Carolina, Columbia.

Jaeger, J. C., and N. G. W. Cook (1969). *Fundamentals of Rock Mechanics*, Methuen, London, 11–281.

Jost, M. L., T. Büßelberg, Ö. Jost, and H.-P. Harjes (1998). Source parameters of injection-induced microearthquakes at 9 km depth at the KTB deep drilling site, Germany, *Bull. Seism. Soc. Am.* **88,** 815–832.

Kessels, W., and J. Kück (1995). Hydraulic communication in crystalline rock between the two boreholes of the Continental Deep Drilling Project in Germany, *Int. J. Rock Mech. Min. Sci. Geomech. Abstr.* **32,** 37–47.

Lee, W. H. K., and J. C. Lahr (1972). HYPO71: a computer program for determining hypocenter, magnitude, and first motion pattern of local earthquakes, *U.S. Geol. Surv. Open-File Rept. 75–311*, 113 pp.

McGarr, A. (1994). Some comparisons between mining-induced and laboratory earthquakes, *Pageoph* **142,** 467–489.

McGarr, A., and G. A. Wiebols (1977). Influence of mine geometry and closure volume on seismicity in a deep-level mine, *Int. J. Rock Mech. Min. Sci. Geomech. Abstr.* **14,** 139–145.

Rajendran, K., and P. Talwani (1992). The role of elastic, undrained and drained responses in triggering earthquake at Monticello Reservoir, South Carolina, *Bull. Seism. Soc. Am.* **82,** 1867–1888.

Secor, D. T. Jr., L. S. Peck, D. M. Pitcher, D. C. Prowell, D. H. Simpson, W. A. Smith, and A. W. Snoke (1982). Geology of the area of induced seismic activity at Monticello Reservoir, South Carolina, *J. Geophys. Res.* **87,** 6945–6957.

Seeburger, D. A., and M. D. Zoback (1982). The distribution of natural fractures and joints at depth in crystalline rock, *J. Geophys. Res.* **87,** 5517–5534.

Segall, P. (1989). Earthquakes triggered by fluid extraction, *Geology* **17,** 942–946.

Simpson, D. W., and S. K. Negmatullaev. (1981). Induced seismicity at Nurek Reservoir, *Bull. Seism. Soc. Am.* **71,** 1561–1586.

Simpson, D. W., W. S. Leith, and C. H., Scholz (1988). Two types of reservoir induced seismicity, *Bull. Seism. Soc. Am.* **78,** 2025–2040.

Skempton, A. W. (1954). The pore pressure coefficients A and B, *Geotechnique* **4,** 143–147.

South Carolina Electric and Gas Company (1977). Virgil C. Summer Nuclear Station, *Final Safety Analysis Report*, Vol. II, 520 pp.

Talwani, P. (1996). Kaiser effect and reservoir induced seismicity, *EOS Trans. Am. Geophys. Union* **77,** F500.

Talwani, P. (1997). On the nature of reservoir-induced seismicity, *Pageoph* **150,** 473–492.

Talwani, P., and S. Acree (1984). Pore pressure diffusion and the mechanism of reservoir induced seismicity, *Pageoph* **122,** 947–965.

Talwani, P., and S. Acree (1987). Induced seismicity at Monticello Reservoir: a case study, *U.S. Geol. Surv. Final Tech. Rept.*, 271 pp.

Talwani, P., and L. Chen (1998). Are seismogenic faults associated with a characteristic permeability? Introducing, "Seismogenic" permeability, ks, *EOS Trans.* Am. Geophys. Union **79,** F583.

Talwani, P., D. Stevenson, J. Sauber, B. K. Rastogi, A. Drew, J. Chiang, and D. Amick (1978). Seismicity studies at Lake Jocassee, Lake Keowee, and Monticello Reservoir, South Carolina (October 1977-March 1978), *U.S. Geol. Surv. Seventh Tech. Rept.*, 189 pp.

Talwani, P., B. K. Rastogi, and D. Stevenson (1980). Induced seismicity and earthquake prediction studies in South Carolina, *U.S. Geol. Surv. Tenth Tech. Rept.*, 212 pp.

Talwani, P., J. S. Cobb, and M. F. Schaeffer (1999). *In situ* measurement of hydraulic properties of a shear zone in northwestern South Carolina, *J. Geophys. Res.* **104,** 14,993–15,003.

Turcotte, D. L., and G. Schubert (1982). *Geodynamics Application of Continuum Physics to Geological Problems*, John Wiley and Sons, New York, 121–122.

Weast, R. C. (1987). *CRC Handbook of Chemistry and Physics*, CRC Press, Inc., Boca Raton, Florida, F-37.

Zoback, M., and S. Hickman (1982). *In situ* study of the physical mechanisms controlling induced seismicity at Monticello Reservoir, South Carolina, *J. Geophys. Res.* **87,** 6959–6974.

Zoback, M., and H.-P. Harjes (1997). Injection-induced earthquakes and crustal stress at 9 km depth at the KTB deep drilling site, Germany, *J. Geophys. Res.* **102,** 18,477–18,491.

Appendix I

The elastic (undrained) stress changes at the hypocenter of event 20 due to water-level change in each grid block were calculated using equation (2). The sum of the stress components for all the blocks gave the components of the total stress change.

Appendix II

Pore pressure increase due to diffusion at the hypocenter of event 20 was calculated for increase in water level at each day before the event (Table A2). The sum of pore pressure increase over the 26-step water-level increase was used to calculate ΔS.

Table A1
Changes in Elastic (Undrained) Stress Components due to the Loading of Each Grid Block

Block No.	Δh (m)	A (km²)	r (km)	σxx	σyy	σzz	τxy	τxz	τyz
5	7.63	0.15	5.85	0.11	0.26	0.05	0.06	0.02	0.15
6	4.58	0.10	5.99	0.04	0.10	0.02	0.01	0.00	0.05
9	4.58	0.05	4.61	0.03	0.12	0.03	0.02	0.01	0.08
10	9.15	0.45	4.98	0.45	1.60	0.39	0.27	0.11	0.98
13	12.20	0.70	4.06	0.94	6.11	2.26	0.96	0.49	4.42
14	7.63	0.25	4.14	0.21	1.31	0.46	0.15	0.08	0.93
16	9.15	0.20	3.40	0.47	1.75	1.17	1.08	0.76	1.66
17	13.73	0.90	3.22	1.12	15.46	10.37	3.98	2.82	14.66
18	10.68	0.20	3.04	0.08	3.08	2.41	0.51	0.39	3.14
20	7.63	0.15	2.78	0.61	1.29	2.05	1.24	1.34	1.89
21	16.78	0.70	3.05	0.64	16.60	13.01	3.69	2.83	16.96
22	16.78	0.90	2.49	−0.12	25.48	46.23	10.93	12.57	40.20
23	13.73	0.25	2.71	2.43	3.33	6.94	4.00	4.91	5.66
24	4.58	0.05	2.23	0.36	−0.05	1.29	0.18	0.84	0.28
25	10.68	0.40	1.97	−0.61	−0.61	41.98	3.10	11.41	11.41
26	16.78	0.90	1.97	−2.14	−2.14	148.42	10.97	40.35	40.33
27	10.68	0.75	2.37	13.07	−0.30	32.05	6.63	24.40	8.71
28	4.58	1.00	2.93	0.13	0.01	0.12	0.05	0.15	0.04
29	13.73	0.15	2.16	2.89	−0.70	12.77	1.25	7.64	2.08
30	16.78	0.80	1.97	−1.91	−1.91	131.93	9.75	35.87	35.85
31	19.83	1.00	1.97	−2.81	−2.81	194.89	14.40	52.99	52.96
32	13.73	0.60	2.43	13.69	−0.18	28.67	6.35	23.38	7.79
33	13.73	0.40	2.97	8.12	0.24	6.92	1.88	8.66	1.50
34	19.83	0.85	2.35	−2.19	27.81	68.13	11.28	14.82	51.84
35	19.83	1.00	2.37	−0.74	31.94	78.31	16.20	21.29	59.58
36	18.30	1.00	2.76	16.25	14.00	33.67	20.90	27.46	25.62
37	12.20	0.50	3.29	5.92	1.97	4.62	4.26	6.03	3.26
38	19.83	0.75	3.05	0.75	19.40	15.20	4.31	3.31	19.83
39	15.25	0.95	3.10	1.95	18.77	14.71	7.30	5.60	19.18
40	13.73	0.80	3.38	4.12	9.43	7.33	7.80	5.98	9.56
41	7.63	0.05	3.88	0.06	0.08	0.05	0.08	0.06	0.07
42	13.73	0.20	3.61	0.24	2.71	1.31	0.24	0.14	2.21
43	10.68	0.25	3.61	0.24	2.65	1.28	0.23	0.14	2.16
44	7.63	0.20	4.03	0.40	0.88	0.42	0.69	0.41	0.71
Total				65	198	909	155	317	446

All stress components in MPa $\times 10^{-4}$.

Table A2

Pore Pressure Increases due to Diffusion at the Hypocenter for Different Hydraulic Diffusivities Caused by the Reservoir
Water-Level Changes Each Day

i	h_i (m)	t_i (days)	R_i (km)	$(\Delta P_{\text{diff}})_i$ (MPa $\times 10^{-4}$)		
				$C = 0.5$ m²/sec	$C = 2$ m²/sec	$C = 5$ m²/sec
1	0.61	41	1.91	18.44	36.71	44.91
2	1.22	40	1.91	36.16	72.88	89.46
9	0.30	33	1.91	7.63	17.14	21.62
10	0.91	32	1.91	22.23	50.89	64.50
11	1.22	31	1.91	28.72	67.11	85.47
12	1.52	30	1.88	35.63	83.65	106.68
13	1.52	29	1.88	34.41	82.64	105.97
14	1.22	28	1.88	26.54	65.26	84.18
18	0.61	24	1.86	11.40	30.97	40.91
19	0.91	23	1.86	16.25	45.64	60.79
20	1.22	22	1.86	20.48	59.70	80.22
21	1.22	21	1.85	19.64	58.87	79.62
22	1.22	20	1.85	18.39	57.58	78.68
23	0.91	19	1.85	12.83	42.16	58.26
28	0.30	14	1.85	2.58	11.93	17.81
29	0.91	13	1.85	6.71	34.19	52.19
30	0.61	12	1.85	3.78	21.63	33.87
31	0.91	11	1.85	4.66	30.54	49.25
32	0.61	10	1.85	2.45	18.96	31.66
35	0.30	7	1.85	0.41	6.88	13.49
36	0.61	6	1.85	0.45	11.60	24.84
37	0.61	5	1.85	0.19	9.20	22.22
38	0.61	4	1.84	0.06	6.65	19.09
39	0.61	3	1.84	0.01	3.85	14.87
40	0.30	2	1.84	5.54E−5	0.66	4.65
41	0.30	1	1.84	2.04E−10	0.03	1.26
Sum				330	930	1285

Department of Geological Sciences
University of South Carolina
701 Sumter Street, EWSC Room 517
Columbia, South Carolina 29208
lychen@prithvi.seis.sc.edu
talwani@prithvi.seis.sc.edu